SCIENCE CHINA
Information Sciences

December 2019, Vol. 62 220405:1–220405:8
https://doi.org/10.1007/s11432-019-1472-6

• RESEARCH PAPER •
Special Focus on Two-Dimensional Materials and Device Applications

A study on ionic gated MoS_2 phototransistors

Binmin WU[2,1,4†], Xudong WANG[1†], Hongwei TANG[3†], Tie LIN[1], Hong SHEN[1], Weida HU[1], Xiangjian MENG[1], Wenzhong BAO[3*], Jianlu WANG[1*] & Junhao CHU[2,1]

[1]*State Key Laboratory of Infrared Physics, Shanghai Institute of Technical Physics, Chinese Academy of Sciences, Shanghai* 200083*, China;*
[2]*School of Physical Science and Technology, ShanghaiTech University, Shanghai* 201210*, China;*
[3]*State Key Laboratory of ASIC and System, School of Microelectronics, Fudan University, Shanghai* 200433*, China;*
[4]*University of Chinese Academy of Sciences, Beijing* 100049*, China*

Received 2 June 2019/Revised 18 July 2019/Accepted 24 July 2019/Published online 31 October 2019

Abstract Molybdenum disulfide (MoS_2) holds great promise in the future applications of nanoelectronics and optoelectronic devices. Exploring those interesting physical properties of MoS_2 using a strong electric field provided by electrolyte-gel is a robust approach. Here, we fabricate an MoS_2 phototransistor gated by electrolyte-gel which is located on a fused silica substrate. Under the modulation of electrolyte-gel, the Schottky barrier between MoS_2 and source/drain electrodes can be widely regulated from 11 to 179 meV. The MoS_2 phototransistor exhibits excellent responsivity of 2.68×10^4 A/W and detectivity of 9.6×10^{10} Jones under visible incident light at negative gate voltage modulation. We attribute the optoelectronic performance enhancement to the Schottky barrier modulation of electrolyte-gel gating. It makes the device suitable for applications in high-sensitive photodetectors.

Keywords MoS_2 phototransistor, electrolyte-gel gating, Schottky barrier, electric double layer, two-dimensional materials

Citation Wu B M, Wang X D, Tang H W, et al. A study on ionic gated MoS_2 phototransistors. Sci China Inf Sci, 2019, 62(12): 220405, https://doi.org/10.1007/s11432-019-1472-6

1 Introduction

Two-dimensional materials have become an essential research object in electronics and optoelectronics [1, 2], since they are constantly breaking through the limits of devices based on those traditional materials. In view of the new features of 2D materials, it can also be widely used in electrocatalysis, gas sensors, pressure sensors and energy [3–6]. Graphene is the first 2D material discovered [7, 8], however, the absence of bandgap is its major drawback which hinders the applications in logic electronics. Molybdenum disulfide (MoS_2) is one of the most typical transition-metal dichalcogenides (TMDs) which embraces a considerable bandgap. The bandgap of MoS_2 changes from 1.2 eV in bulk to 1.8 eV in monolayer [9–11]. Based on its excellent physical properties, MoS_2 has displayed great potential in ultralow-power nanoelectronics [12–14], optoelectronics [15, 16], and transducers [17–21]. It is usually assembled into a heterojunction using two-dimensional materials and other-dimensional materials, which can greatly improve the photodetection performance of 2D materials [22–26]. However, the performance of MoS_2 phototransistors fabricated on Si/SiO_2 substrate is commonly limited by the interface defects, as the same case of its mobility. Actually, under the modulation of high-k dielectrics, such as HfO_2, Al_2O_3, and ferroelectrics [27–32], the charge impurities are screened and then the scattering at the interface between MoS_2 and dielectric is reduced.

* Corresponding author (email: baowz@fudan.edu.cn, jlwang@mail.sitp.ac.cn)
† Wu B M, Wang X D, and Tang H W have the same contribution to this work.

As a result, the substantial mobility and optoelectronic performance are both enhanced. Another factor limiting device performance is the contact between MoS_2 and source/drain electrodes [33]. It should be admitted that the linear output curves in most field effect transistors (FETs) cannot prove to be Ohmic contact. Numerous methods have been developed to eliminate the Schottky barrier, such as using low work function contact metals [33, 34], forming a tunneling contact [35], and phase-engineered low-resistance contacts [36]. For photodetectors, Schottky barrier in a device is an effective approach to reduce the dark current, improve the photocurrent gain, and achieve fast photoresponse speed [37, 38]. The height of the Schottky barrier can be modulated by applying a gate voltage. In order to achieve a wide range modulation of Schottky barrier, it is necessary to employ a gate dielectric with large capacitance. Electrolyte-gel can form electric double layers and thus act as an extremely large capacitance. The MoS_2 FETs gated by electrolyte-gel exhibit high carrier mobility, high current on/off ratio, and low subthreshold swing. Moreover, the Schottky barrier can be dramatically modulated and the MoS_2 FETs can be transferred into bipolar characteristic [39].

In this study, we report an MoS_2 phototransistor gated by electrolyte-gel to modulate the Schottky barrier and enhance its optoelectronic performance. Although the output curves of MoS_2 FETs have a good linear characteristic, the existence of the Schottky barrier between MoS_2 and the source/drain electrodes can be determined in the photocurrent mapping. The Schottky barrier height changes from 11 to 179 meV with the modulation of electrolyte-gel. Under the visible incident light, the MoS_2 phototransistor exhibits high responsivity of 2.68×10^4 A/W and detectivity of 9.6×10^{10} Jones at -3 V gate voltage gating, indicating that the sensitivity of the photodetector is effectively enhanced by electrolyte-gel modulation.

2 Device structure and preparation

Figure 1(a) shows a three-dimensional structure schematic of the MoS_3 phototransistor with electrolyte-gel gating. The device is fabricated on a highly transparent fused silica substrate which transmittance for visible light is greater than 95%. Few-layer MoS_2 is mechanically exfoliated from bulk crystals and served as the channel. The source and drain electrodes are prepared by electron beam lithography, thermal evaporation and lift-off processes. Meanwhile, the side gate electrode is also prepared at this step. The electrode metal is titanium/gold (Ti/Au), and the thickness of Ti and Au is 15 and 45 nm, respectively. At last, the electrolyte-gel covers the surface of MoS_2 channel and all electrodes by dropping method. The electrolyte-gel is composed of lithium perchlorate ($LiClO_4$) dissolved in high-molecular-weight polyethylene oxide (PEO). Specifically, 0.5 g PEO and 0.06 g $LiClO_4$ are dissolved in 18 mL methanol. Then the solution is stirred for 30 min when heated to 70°C. Using Buchner funnel together with 15 μm filter paper, the large particles are removed and the solution becomes more transparent, more methanol is added to adjust the viscosity of the electrolyte. Finally, the obtained $LiClO_4$/PEO electrolyte is then continuously stirred in a glass bottle to keep the suspension homogeneous. As the top view of the device covered with the electrolyte-gel does not clearly show its structure, Figure 1(b) displays the micrograph of the device before covering the electrolyte-gel. The thickness of MoS_2 is further confirmed by atomic force microscopy (AFM) and Raman spectroscopy. As shown in Figure 1(c), the thickness of MoS_2 is approximately 22 nm. Moreover, the Raman shift difference between E^1_{2g} and A_{1g} is 25.1 cm^{-1} (Figure 1(d)), which also indicates that the MoS_2 used in this study is a few-layer sample [40].

3 Electrical characteristic and working principle

Before the optoelectronic measurements, we first study the electrical properties and working principle of the device. The electrical measurements are carried out by an Agilent B1500 semiconductor analyzer with a Lakeshore probe station under high vacuum (2×10^{-4} Torr). The vacuum environment is very important for preventing the effects of water in the air to electrolyte-gel properties. Figure 2(a) shows

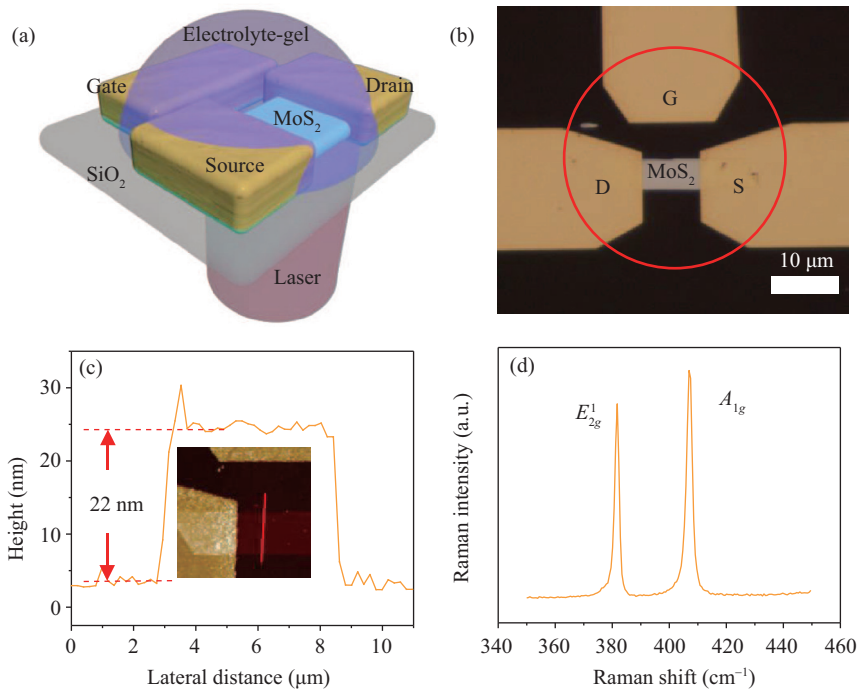

Figure 1 (Color online) Device structure and characteristics of MoS_2. (a) A three-dimensional structure diagram of the MoS_2 phototransistor with electrolyte-gel gating. (b) Micrograph of an MoS_2 transistor with a side gate prepared on the fused silica substrate. The area circled by the red ellipse will be covered by electrolyte-gel. (c) The height of MoS_2 used as the channel is approximately 22 nm, the inset is the AFM morphology of the device. (d) Raman spectrum of MoS_2 on the fused silica substrate with two vibration modes E^1_{2g} and A_{1g} (the laser excitation wavelength is 532 nm).

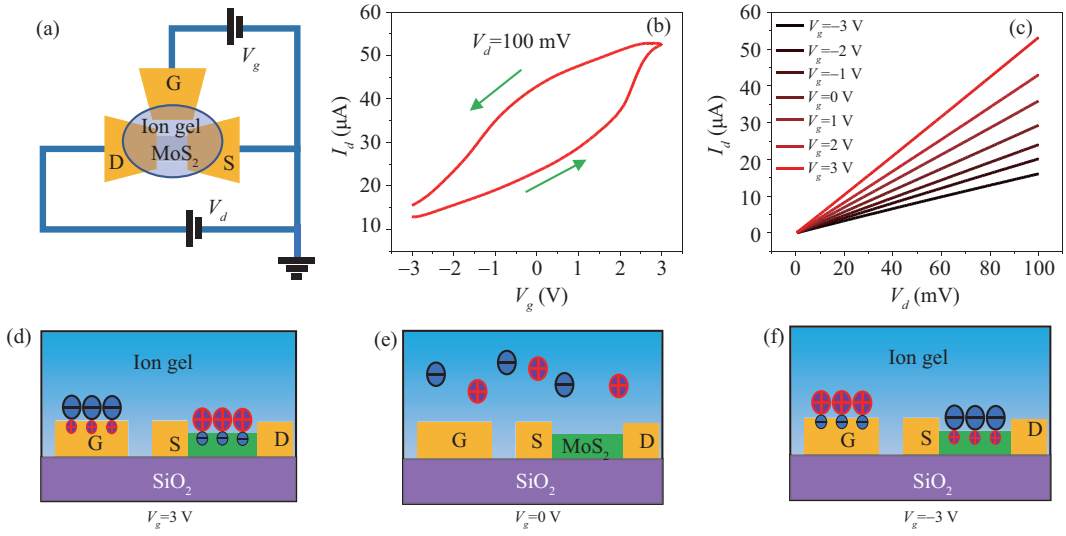

Figure 2 (Color online) Electrical characteristics and working principle of the device. (a) A working circuit schematic of the MoS_2 phototransistor with electrolyte-gel gating; (b) the transfer curves of the device at 100 mV drain bias; (c) the output characteristics of the device with gate voltage varies from −3 V to 3 V; (d)–(f) schematics of device working principle at positive, zero and negative gate voltage. When $V_g \neq 0$ V, an electric-double layer is formed at the surface of the side gate electrode and the MoS_2 channel.

the schematic of the electrical measurement circuit. The gate voltage (V_g) is applied between the gate and the source electrode, then acts on the electrolyte-gel to modulate the MoS_2 channel. The drain bias is applied between the drain and the source electrode, which is used to read the channel current. Figure 2(b) demonstrates the transfer curve of the device at $V_d = 100$ mV. Figure 2(c) shows the output

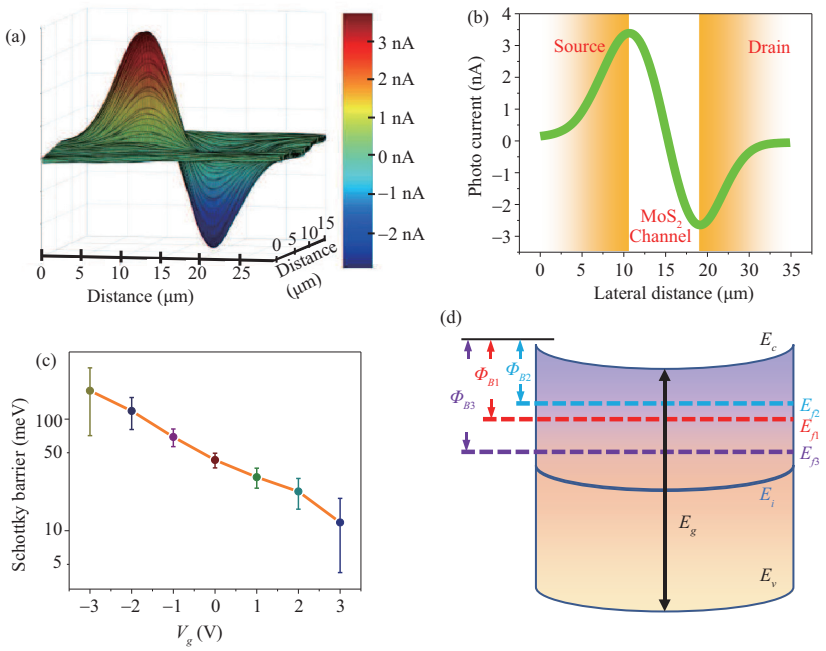

Figure 3 (Color online) Schottky barrier modulation of electrolyte-gel gating. (a) The photocurrent mapping of the MoS_2 phototransistor covered with electrolyte-gel and the $V_g = 0$ V, $V_d = 0$ V. Significant photocurrent generation can be found at the contact between MoS_2 channel and source/drain electrode. Red and blue color represent positive and negative photocurrent, respectively. (b) A section cut perpendicular to the plane along two extreme points in (a). It is apparent that a photocurrent is generated at the position of Schottky barrier. (c) Schottky barrier height and standard deviation of the device at different gate voltages. (d) The band structure of MoS_2 at $V_g = 3$ V, $V_g = 0$ V, $V_g = -3$ V. The drain bias is 0 V in all cases. ϕ_{B1}, E_{f1}, ϕ_{B2}, E_{f2}, ϕ_{B3}, E_{f3} correspond to Schottky barrier height and Fermi level at $V_g = 3$ V, $V_g = 0$ V, $V_g = -3$ V, respectively. E_c, E_v, E_i, and E_g represent the conduction band, valence band, intrinsic Fermi level and band gap of MoS_2, respectively.

curves of the device at V_g from -3 to 3 V. Such a linear trend is usually considered to be Ohmic contact between source/drain electrode and MoS_2.

Figure 2(d)–(e) demonstrates the schematic illustration of the device working principle. As shown in Figure 2(d), ions are randomly distributed in the electrolyte-gel at $V_g = 0$ V. When a positive V_g is applied on the gate electrode, such as $V_g = 3$ V (Figure 2(e)), negative ions accumulate on the gate electrode side and positive ions accumulate on the MoS_2 side. Conversely, the positive and negative ions in electrolyte-gel are reversed by negative gate voltage (Figure 2(f)). In both Figure 2(e) and (f), electric double layers form at the interfaces between electrolyte-gel and gate electrode and between electrolyte-gel and MoS_2. Therefore, the number of ions in the electric double layer changes with the variation of gate voltage, thereby modulating the carriers in MoS_2 channel.

4 Optoelectronic performance and the Schottky barrier modulation of electrolyte-gel gating

We further explore the optoelectronic properties of the device. Figure 3(a) demonstrates the three-dimensional photocurrent mapping profile of the device at $V_g = 0$ V and $V_d = 0$ V. The incident light wavelength is 520 nm and power is 16.3 μW. A curve along the peaks of the photocurrent is extracted, as shown in Figure 3(b). The position of the device corresponding to the photocurrent is also marked in Figure 3(b). It is obvious that most of the photocurrent occurs in the contact area between MoS_2 and metal electrodes. Moreover, the photocurrent directions of these two contact areas are the opposite. Therefore, it indicates that the Schottky barrier exists between MoS_2 and electrodes, and the photocurrent is derived from the photovoltaic effect.

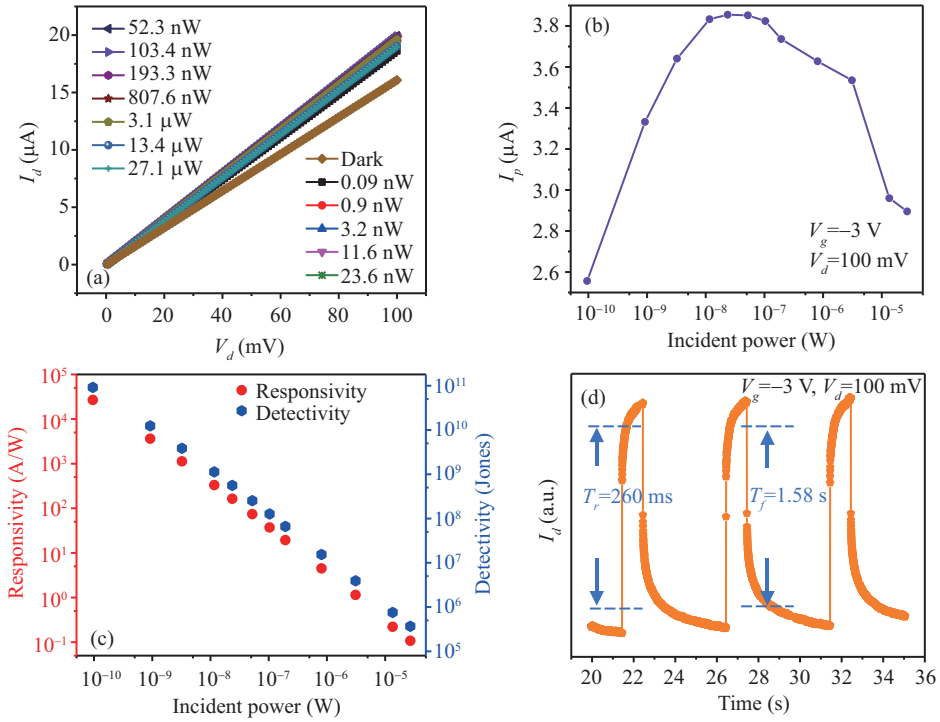

Figure 4 (Color online) Optoelectronic performance of the MoS_2 phototransistor gated by electrolyte-gel. (a) I_d-V_d characteristics of the device with $V_g = -3$ V under dark and different laser powers (the laser wavelength is 520 nm and the power varies from 0.09 nW to 27.1 μW); (b) the photocurrent dependence on the incident laser power; (c) the responsivity and detectivity of the device at different incident light powers; (d) the photocurrent rise and fall time of the device at $V_g = -3$ V and $V_d = 100$ mV.

The height of the Schottky barrier can be calculated by [33, 41]

$$I = AA^*T^2 \exp\left(\frac{-q\phi_B}{k_B T}\right), \tag{1}$$

where I is the current flowing through the device, A is the area of the Schottky junction, A^* is the effective Richardson constant, q is the elementary charge, k_B is the Boltzmann constant, and T is the temperature. Here, we conduct electrical measurements with different temperatures on five samples. Under the modulation of different gate voltages, the temperature dependence of I_d-V_d is shown in Figures S1–S5. According to (1), we extract the height of Schottky barriers from these I_d-V_d curves at different gate voltages, as shown in Figure 3(c). The curve in Figure 3(c) is the standard deviation of the height of Schottky barriers at different gate voltages. It is well known that the Schottky barrier can be modulated by the gate voltage, however, such a large barrier modulation range benefits from the strong electric field provided by electrolyte-gel. The band diagram of MoS_2 modulated by gate voltage is shown in Figure 3(d). When $V_g = 0$ V, MoS_2 is in the initial state and its Fermi level (E_{f1}) is close to the conduction band (E_c). Based on our experimental results, the Schottky barrier height is approximately 43 meV at $V_g = 0$ V ($\phi_{B1} \approx 43$ meV). When V_g is increased to 3 V, the Fermi level is elevated by this positive gate voltage to a position (E_{f2}) closer to the conduction band. The Schottky barrier height is thereby decreased to about 11 meV ($\phi_{B2} \approx 11$ meV).

Conversely, the Fermi level is degraded by negative gate voltage ($V_g = -3$ V) to a position (E_{f3}) closer to the central level (E_i). In this case, the Schottky barrier height (ϕ_{B3}) exceeds 179 meV. Moreover, other studies had demonstrated that under the modulation of ionic liquids, the Fermi level of MoS_2 can be degraded below the central level to achieve a bipolar MoS_2 [39].

Photodetectors based on Schottky barrier have advantages of fast photoresponse speed, low power consumption, and high photocurrent gain [37,38]. We comprehensively study the optoelectronic performance of MoS_2 gated by electrolyte-gel. As shown in Figure 4(a), with the modulation of −3 V gate voltage,

we measure the output characteristics of the device at different incident light powers. In this case, the wavelength of incident light is 520 nm. For a clear display of the dependence of the photocurrent of the device on the incident light power, we extract the photocurrent at $V_d = 100$ mV as shown in Figure 4(b). Obviously, the relationship between photocurrent and incident light power is a nonlinear curve similar a parabola. Such a phenomenon is abnormal compared to photoconductive and Schottky junction photodetectors [42]. This abnormality is mainly attributed to the ion intercalation effect. Actually, during the optoelectronic measurements, we gradually increase the incident light power from 0.09 nW to 27.1 μW, it takes about 73 s to obtain each curve in Figure 4(a). The intercalation effect of electrolyte-gel on MoS_2 exacerbates with time, especially under a high gate voltage. The interlaminar molecular structure of MoS_2 is destroyed, causing the photocurrent to degrade as the incident light power increases after a period of time. The responsivity (R) and detectivity (D^*) can be calculated by $R = I_p/P$, and $D^* = \sqrt{RA/(2eI_{\rm dark})}$, where I_p is the photocurrent, P is the power of incident light, A is the area of the detector, e is the unit charge, and $I_{\rm dark}$ is the dark current. Figure 4(c) demonstrates the incident light power dependence of the responsivity and detectivity of the device. The responsivity is 2.68×10^4 A/W and detectivity of 9.6×10^{10} Jones when the incident light power is 0.09 nW. The photocurrent switching characteristic of the device at $V_g = -3$ V and $V_d = 100$ mV is shown in Figure 4(d). It can be extracted that the rise and fall times of the photocurrent are 260 ms and 1.58 s, respectively. The photoresponse speed is still faster than that of MoS_2 phototransistor gated by SiO_2. Moreover, Figure S6 demonstrates the photocurrent switching characteristic of the device at $V_g = -3$ V and $V_d = 0$ V with a laser power of 96 μW. Based on the photovoltaic effect of Schottky junction, the device also embraces an obvious photoresponse with the visible light.

5 Conclusion

In conclusion, we studied the optoelectronic properties of MoS_2 phototransistor gated by electrolyte-gel. The Schottky barrier between MoS_2 and the source/drain electrodes is greatly modulated by the strong electric field provided by electrolyte-gel. Through the temperature dependence experiments, we accurately calculate the height of the Schottky barrier and describe its modulation principle of electrolyte-gel. The photocurrent mapping indicates that the photocurrent of the device is mainly induced by the Schottky junction. As a photodetector, the high responsivity of 2.68×10^4 A/W and detectivity of 9.6×10^{10} Jones are achieved. Electrolyte-gel is useful in exploring the ultimate physical properties of semiconductors. MoS_2 phototransistor gated by electrolyte-gel is promising in photodetector applications with high sensitivity.

Acknowledgements This work was partially supported by Major State Basic Research Development Program (Grant Nos. 2016YFB0400801), National Natural Science Foundation of China (Grant Nos. 61722408, 61835012, 51802041), Key Research Project of Frontier Sciences of Chinese Academy of Sciences (Grant Nos. QYZDY-SSW-JSC042, QYZDB-SSW-JSC016), National Postdoctoral Program for Innovative Talents (Grant No. BX20180329), and Shanghai Sailing Program (Grant No. 19YF1454900).

Supporting information Figures S1–S6. The supporting information is available online at info.scichina.com and link.springer.com. The supporting materials are published as submitted, without typesetting or editing. The responsibility for scientific accuracy and content remains entirely with the authors.

References

1 Wang X D, Liu C S, Chen Y, et al. Ferroelectric FET for nonvolatile memory application with two-dimensional $MoSe_2$ channels. 2D Mater, 2017, 4: 025036
2 Chen Y, Wang X D, Wang P, et al. Optoelectronic properties of few-layer MoS_2 FET gated by ferroelectric relaxor polymer. ACS Appl Mater Interfaces, 2016, 8: 32083–32088
3 Lan C Y, Zhou Z Y, Wei R J, et al. Two-dimensional perovskite materials: from synthesis to energy-related applications. Mater Today Energy, 2019, 11: 61–82
4 Alarawi A, Ramalingam V, He J H. Recent advances in emerging single atom confined two-dimensional materials for water splitting applications. Mater Today Energy, 2019, 11: 1–23

5 Ai Y, Hsu T H, Wu D C, et al. An ultrasensitive flexible pressure sensor for multimodal wearable electronic skins based on large-scale polystyrene ball@reduced graphene-oxide core-shell nanoparticles. J Mater Chem C, 2018, 6: 5514–5520
6 Medina H, Li J G, Su T Y, et al. Wafer-scale growth of WSe_2 monolayers toward phase-engineered hybrid WOx/WSe_2 films with sub-ppb NOx gas sensing by a low-temperature plasma-assisted selenization process. Chem Mater, 2017, 29: 1587–1598
7 Novoselov K S, McCann E, Morozov S V, et al. Unconventional quantum Hall effect and Berry's phase of 2π in bilayer graphene. Nat Phys, 2006, 2: 177–180
8 Schedin F, Geim A K, Morozov S V, et al. Detection of individual gas molecules adsorbed on graphene. Nat Mater, 2007, 6: 652–655
9 Mak K F, Lee C, Hone J, et al. Atomically thin MoS_2: a new direct-gap semiconductor. Phys Rev Lett, 2010, 105: 136805
10 Naber R C G, Tanase C, Blom P W M, et al. High-performance solution-processed polymer ferroelectric field-effect transistors. Nat Mater, 2005, 4: 243–248
11 Chang Y H, Zhang W J, Zhu Y H, et al. Monolayer $MoSe_2$ grown by chemical vapor deposition for fast photodetection. ACS Nano, 2014, 8: 8582–8590
12 Tian B B, Liu L, Yan M G, et al. A robust artificial synapse based on organic ferroelectric polymer. Adv Electron Mater, 2019, 5: 1800600
13 Wang J L, Hu W D. Recent progress on integrating two-dimensional materials with ferroelectrics for memory devices and photodetectors. Chin Phys B, 2017, 26: 037106
14 Wang X D, Chen Y, Wu G J, et al. Two-dimensional negative capacitance transistor with polyvinylidene fluoride-based ferroelectric polymer gating. npj 2D Mater Appl, 2017, 1: 38
15 Lopez-Sanchez O, Lembke D, Kayci M, et al. Ultrasensitive photodetectors based on monolayer MoS_2. Nat Nanotech, 2013, 8: 497–501
16 Wang X D, Wang P, Wang J L, et al. Ultrasensitive and broadband MoS_2 photodetector driven by ferroelectrics. Adv Mater, 2015, 27: 6575–6581
17 Gao G Y, Wan B S, Liu X Q, et al. Tunable tribotronic dual-gate logic devices based on 2D MoS_2 and black phosphorus. Adv Mater, 2018, 30: 1705088
18 Park M, Park Y J, Chen X, et al. MoS_2-based tactile sensor for electronic skin applications. Adv Mater, 2016, 28: 2556–2562
19 Kim J S, Yoo H W, Choi H O, et al. Tunable volatile organic compounds sensor by using thiolated ligand conjugation on MoS_2. Nano Lett, 2014, 14: 5941–5947
20 Perkins F K, Friedman A L, Cobas E, et al. Chemical vapor sensing with monolayer MoS_2. Nano Lett, 2013, 13: 668–673
21 Jin K, Xie L M, Tian Y, et al. Au-modified monolayer MoS_2 sensor for DNA detection. J Phys Chem C, 2016, 120: 11204–11209
22 Gao N, Fang X S. Synthesis and development of graphene-inorganic semiconductor nanocomposites. Chem Rev, 2015, 115: 8294–8343
23 Liu S X, Zheng L X, Yu P P, et al. Novel composites of α-Fe_2O_3 tetrakaidecahedron and graphene oxide as an effective photoelectrode with enhanced photocurrent performances. Adv Funct Mater, 2016, 26: 3331–3339
24 Ouyang W X, Teng F, Fang X S. High performance BiOCl nanosheets/TiO_2 nanotube arrays heterojunction UV photodetector: the influences of self-induced inner electric fields in the BiOCl nanosheets. Adv Funct Mater, 2018, 28: 1707178
25 Tang S Y, Medina H, Yen Y T, et al. Enhanced photocarrier generation with selectable wavelengths by M-decorated-CuInS2 nanocrystals (M=Au and Pt) synthesized in a single surfactant process on MoS_2 Bilayers. Small, 2019, 15: 1803529
26 Yang W, Chen J X, Zhang Y, et al. Silicon-compatible photodetectors: trends to monolithically integrate photosensors with chip technology. Adv Funct Mater, 2019, 29: 1808182
27 Kc S, Longo R C, Wallace R M, et al. Computational study of MoS_2/HfO_2 defective interfaces for nanometer-scale electronics. ACS Omega, 2017, 2: 2827–2834
28 Song J G, Kim S J, Woo W J, et al. Effect of Al_2O_2 deposition on performance of top-gated monolayer MoS_2-based field effect transistor. ACS Appl Mater Interfaces, 2016, 8: 28130–28135
29 Yin C, Wang X D, Chen Y, et al. A ferroelectric relaxor polymer-enhanced p-type WSe_2 transistor. Nanoscale, 2018, 10: 1727–1734
30 Tu L Q, Wang X D, Wang J L, et al. Ferroelectric negative capacitance field effect transistor. Adv Electron Mater, 2018, 4: 1800231
31 Wang J L, Fang H H, Wang X D, et al. Recent progress on localized field enhanced two-dimensional material photodetectors from ultraviolet-visible to infrared. Small, 2017, 13: 1700894
32 Xue S, Zhao X L, Wang J L, et al. Preparation of $La_{0.67}Ca_{0.23}Sr_{0.1}MnO_3$ thin films with interesting electrical and magnetic properties via pulsed-laser deposition. Sci China Phys Mech Astron, 2017, 60: 027521
33 Liu Y, Guo J, Zhu E B, et al. Approaching the Schottky-Mott limit in van der Waals metal-semiconductor junctions. Nature, 2018, 557: 696–700
34 Guo R, You L, Zhou Y, et al. Non-volatile memory based on the ferroelectric photovoltaic effect. Nat Commun, 2013, 4: 1990
35 Wang J, Yao Q, Huang C W, et al. High mobility MoS_2 transistor with low Schottky barrier contact by using atomic

thick h-BN as a tunneling layer. Adv Mater, 2016, 28: 8302–8308
36 Kappera R, Voiry D, Yalcin S E, et al. Phase-engineered low-resistance contacts for ultrathin MoS_2 transistors. Nat Mater, 2014, 13: 1128–1134
37 Osinsky A, Gangopadhyay S, Lim B W, et al. Schottky barrier photodetectors based on AlGaN. Appl Phys Lett, 1998, 72: 742–744
38 Yang Y B, Huang L, Xiao Y, et al. Tunable polarity behavior and high-performance photosensitive characteristics in Schottky-barrier field-effect transistors based on multilayer WS_2. ACS Appl Mater Interfaces, 2018, 10: 2745–2751
39 Zhang Y J, Ye J T, Matsuhashi Y, et al. Ambipolar MoS_2 thin flake transistors. Nano Lett, 2012, 12: 1136–1140
40 Li H, Zhang Q, Yap C C R, et al. From bulk to monolayer MoS_2: evolution of Raman scattering. Adv Funct Mater, 2012, 22: 1385–1390
41 Das S R, Kwon J, Prakash A, et al. Low-frequency noise in $MoSe_2$ field effect transistors. Appl Phys Lett, 2015, 106: 083507
42 Chen Y, Wang X D, Wu G J, et al. High-performance photovoltaic detector based on $MoTe_2/MoS_2$ van der Waals heterostructure. Small, 2018, 14: 1703293